Metal–Metal Interactions in Tetrakis(diphenylphosphino)benzene-Bridged Dimetallic Complexes and Their Related Coordination Polymers

Pei-Wei Wang and Marye Anne Fox*

Department of Chemistry and Biochemistry, University of Texas, Austin, Texas 78712

Received November 24, 1993®

Electrochemical, EPR, and spectroelectrochemical methods have been used to probe electronic coupling through a 1,2,4,5-tetrakis(diphenylphosphino)benzene bridging ligand connecting metal centers in several Ni-, Pd-, and Pt-containing dimetallic complexes. These dimetalated complexes showed weak intervalence charge transfer (IT) bands and slightly shifted redox potentials in comparison with their monometallic models. A Marcus–Hush analysis of the energies of the IT bands for the electrochemically generated mixed-valence heterodimetallic complexes (Ni^0–Pd^{II} and Ni^0–Pt^{II}, respectively) established the magnitude of intermetallic electronic coupling. The weak thermal coupling observed in these dimetalated complexes is consistent with the very low conductivities (10^{-8}–10^{-10} Ω^{-1} cm^{-1}) observed in the polymeric analogs of these complexes, namely, the newly prepared metal coordination polymers (M = Ni^{II}, Pd^{II}, Pt^{II}) with 1,2,4,5-tetrakis(diphenylphosphino)benzene.

Introduction

Considerable interest has focused on the electronic properties of organometallic polymers,[1] with the expectation that the introduction of transition metal ions into a conjugated polymer chain might lead to partially filled bands and, hence, to significant intrinsic conductivity.[2] Consistent with this theory, metal coordination polymers of tetrathiooxalate,[3] dihydroxybenzoquinone,[4] and benzodithiolene[5] have been reported to exhibit conductivities of 10^{-2}–10^{-4} $(\Omega\ cm)^{-1}$. In order to attain a conductive organometallic coordination polymer, two criteria must be met.[6] First, the redox-active metal centers must be arranged to permit strong metal–metal interaction, which often requires close spatial proximity and similar crystallographic and electronic environments for the metals. Second, the polymers must be partially oxidized or reduced (to a mixed-valence state) to permit free charge transfer along the polymer chain.

The importance of tertiary phosphine ligands in transition-metal coordination chemistry is well-documented.[7] The 1:1 coordination polymer of Ni^{II} with 1,2,4,5-tetrakis(dimethylphosphino)benzene has been shown to have a dark conductivity of 10^{-8} $(\Omega\ cm)^{-1}$ at room temperature.[8] Variation of the complexing metal may have a pronounced effect on the observed conductivity of the analogous coordination polymer because of the difference in dπ(M)–dπ(P) overlap. In this work, the effect of the complexing metal in the series Ni^{II}, Pd^{II}, Pt^{II} on the observed conductivity of polymers **1a–c** has been investigated.

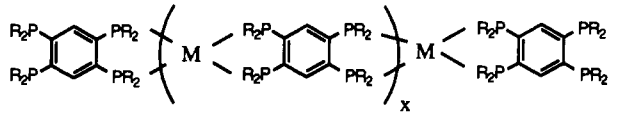

R = Ph

1a M = Ni^{II}

1b M = Pd^{II}

1c M = Pt^{II}

In order to understand the effect of intermetallic electronic coupling on these conductivities, model monometallic $[L_2M^{II}](BF_4)_2$ (L = dppb, dppp) complexes **2–4** and dimetallic [(L)-

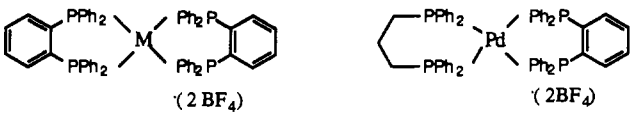

·(2 BF_4)

2a M = Ni^{II}

2b M = Pd^{II}

2c M = Pt^{II}

·(2BF_4)

3

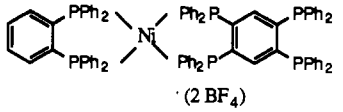

·(2 BF_4)

4

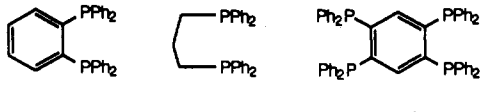

dppb dppp tppb

M^{II}–tppb–M^{II}(L)$](BF_4)_4$ (M = Ni, Pd, Pt; L = dppb, dppp) complexes **5** and **6** were prepared and characterized.

Intermetallic electronic coupling of the dimetallic complexes was investigated by electrochemical, EPR, and spectroelectrochemical methods. The absorption spectra of intervalence charge transfer bands in the mixed-valence heterodimetallic complexes **5d** (Ni^0–Pd^{II}) and **5e** (Ni^0–Pt^{II}) were analyzed by Marcus–Hush

® Abstract published in *Advance ACS Abstracts,* June 1, 1994.

(1) (a) Gutmann, F.; Lyons, L. E. In *Organic Semiconductors;* Kreiger, R. E., Ed. Verlag Chemie: Malabar, FL, 1981; Parts A and B. (b) Meier, H. F. *Organic Semiconductors*; Verlag Chemie: Weinheim, Germany, 1974. (c) Marks, T. J. *Science* **1985**, *227*, 881. (d) Dahm, S.; Strung, W.; Keller, H. J.; Schweitzer, D. *Synth. Met.* **1993**, *55*, 884. (e) Patel, G. C.; Pancholi, H. B.; Patel, M. M. *J. Polym. Mater.* **1991**, *8*, 339. (f) Khandwe, M.; Bajpai, A.; Bajpai, U. D. N. *Macromolecules* **1991**, *24*, 5203. (g) Hassan, M. K.; Abdu-Alla, M. A.; Hasan, R. M. *J. Macromol. Sci.* **1990**, *A27*, 1503.

(2) Gooding, R. D.; Lillya, C. P.; Chien, J. C. W. *J. Chem. Soc., Chem. Commun.* **1983**, 151.

(3) Reynolds, J. R.; Lillya, C. P.; Chien, J. C. W. *Macromolecules* **1987**, *20*, 1184.

(4) Wrobleski, J. T.; Brown, D. B. *Inorg. Chem.* **1979**, *18*, 2738.

(5) Dirk, C. W.; Bousseau, M.; Barrett, P. H.; Moraes, F.; Wudl, F.; Heeger, A. J. *Macromolecules* **1986**, *19*, 266.

(6) Marks, T. J. *Angew. Chem., Int. Ed. Engl.* **1990**, *29*, 857.

(7) McAuliffe, C. A. In *Comprehensive Coordination Chemistry*; Wilkinson, G., Ed.; Pergamon: London, 1987; Vol. 2, pp 989–1066.

(8) Fox, M. A.; Chandler, D. A. *Adv. Mater.* **1991**, *3*, 381.

0020-1669/94/1333-2938$04.50/0

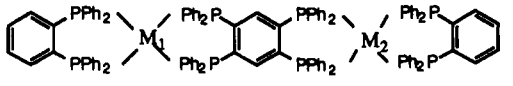

	M_1	M_2
5a	Ni	Ni
5b	Pd	Pd
5c	Pt	Pt
5d	Ni	Pd
5e	Ni	Pt

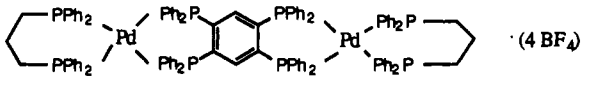

6

theory,[9] allowing us to define the factors influencing the efficiency of thermal electron exchange in these molecules (e.g., reorganization energies, thermal electron transfer rate constants, and activation barriers). These parameters are discussed in relation to the observed order of bulk conductivities of the corresponding metal coordination polymers.

Experimental Section

Physical Measurements. Electrochemical measurements were carried out with a Princeton Applied Research Model 173 potentiostat equipped with a Model 179 digital coulometer and a Model 175 universal programmer or a BAS 100 electrochemical analyzer. Typical experiments were run at 100 mV/s in CH_3CN with 0.1 M tetrabutylammonium hexafluorophosphate. For cyclic voltammetry, a Ag/AgCl wire was used as a pseudo-reference electrode, a Pt wire as the counter electrode, and a Pt disk as the working electrode. Ferrocene was used as an internal standard to calibrate the observed potential (vs SCE).[10] For bulk electrolysis, a Pt flag was used as the working electrode, SCE as the reference electrode, and a carbon cloth as the counter electrode.

EPR spectra of the Ni^I complexes were measured on an IBM ER-300 spectrometer as 0.2 mM solutions in CH_2Cl_2. Proton-decoupled ^{31}P-NMR spectra were measured in CD_3CN or CD_3NO_2 (depending on complex solubility) on a Nicolet NT-360 spectrometer, referenced to a solution of 85% H_3PO_4 in D_2O. Conductivity measurements were made by a previously described two-probe technique[8] on a pressed powder sample in a sandwich cell with a thickness of ~1 mm. (Attempts to prepare crystalline samples of the coordination polymers were unsuccessful.) Ohmic contact was made with silver paint. Near-IR measurements were carried out on a Cary 17 spectrophotometer. Absorption spectra were measured on a Hewlett-Packard 8451A diode array spectrophotometer. Elemental analyses were obtained from the Galbraith Laboratories.

The intervalence charge transfer bands of **5d** (Ni^0–Pd^{II}) and **5e** (Ni^0–Pt^{II}) (Figures 6 and 7, respectively) were deconvoluted with an interactive fitting routine in Spectra-Calc from the Galactic Industries Corp. Two Gaussian curves were used to model the spectra in the range of 400–820 nm. Quality-of-fit was determined by visual inspection of the fitted curve and by a χ^2 error analysis.

Materials. 1,2-Bis(diphenylphosphino)benzene (dppb),[11] 1,2,4,5-tetrakis(diphenylphosphino)benzene (tppb),[11] $[Ni(CH_3CN)_6](BF_4)_2 \cdot {}^1/_2CH_3CN$,[12] $[Pd(CH_3CN)_4](BF_4)_2$,[13] (dppb)$NiCl_2$,[14] (dppb)$PdCl_2$,[15] (dppb)$PtCl_2$,[15] and $[M(dppb)_2](BF_4)_2$[16] (**2a,b**) were prepared by literature methods. (1,5-Cyclooctadiene)platinum(II) chloride ((COD)$PtCl_2$), 4-nitrobenzonitrile, and 1,3-bis(diphenylphosphino)propane (dppp), all from Aldrich, were used as received.

Poly-[Ni^{II}[1,2,4,5-tetrakis(diphenylphosphino)benzene]]$_{37}(BF_4)_{74}$ (1a). A solution of tppb (1 g, 1.23 mmol) in 120 mL of CH_2Cl_2 was added to a solution of $[Ni^{II}(CH_3CN)_6](BF_4)_2 \cdot {}^1/_2CH_3CN$ (613 mg, 1.23 mmol) in 25 mL of CH_3CN. The resulting solution was allowed to stir 24 h at room temperature. The solid product was collected by filtration and purified by Soxhlet extraction with CH_2Cl_2 for 24 h. Yield: 1.02 g (80%). Anal. Calcd for $(C_{54}H_{42}P_4NiB_2F_8)_{37}$: C, 61.94; H, 4.04. Found: C, 60.24; H, 4.13.

End-group analysis was performed by stirring a suspension of the Ni^{II} polymer (200 mg of finely ground powder in 20 mL of CH_2Cl_2) with excess tppb (100 mg in 40 mL of CH_2Cl_2) to cap each metal-terminated polymer chain. After the resulting mixture had been stirred for 24 h at room temperature, the solid product was collected by filtration and washed with CH_2Cl_2. The average number of repeat units can be calculated from the ratio of the integrated peak areas assigned to coordinated and to noncoordinated phosphines in the resulting tppb end-capped polymer **1a**. ^{31}P-NMR (CD_3NO_2): δ 55 (coordinated), –12.5 (end-capped). The integration ratio of coordinated to end-capped phosphines is 37 ± 7, from which the molecular weight is calculated as 39 000 ± 7000.

Poly-[Pd^{II}[1,2,4,5-tetrakis(diphenylphosphino)benzene]]$_{50}(BF_4)_{100}$ (1b). A solution of tppb (1 g, 1.23 mmol) in 100 mL of CH_2Cl_2 was added to a solution of $[Pd(CH_3CN)_4](BF_4)_2$ (545 mg, 1.23 mmol) in 30 mL of CH_3CN. The resulting solution was stirred for 12 h at room temperature. The solid product was collected by filtration, washed with 10 mL of CH_3CN, and purified by Soxhlet extraction with CH_2Cl_2 for 24 h. Yield: 1.02 g (60%). Anal. Calcd for $(C_{54}H_{42}P_4PdB_2F_8)_{50}$: C, 59.24; H, 3.87. Found: C, 58.07; H, 3.83.

End-group analysis as described for the Ni^{II} polymer was performed for the Pd^{II} polymer (a suspension of 1 g of finely ground polymer reacted with 335 mg of tppb in 175 mL of CH_2Cl_2). After the suspension had been stirred for 24 h at room temperature, the solid product was collected by filtration, washed with CH_2Cl_2, and purified by Soxhlet extraction with CH_3CN for 3 h. ^{31}P-NMR (DMSO-d_6): δ 52 (coordinated), –14 (end-capped). The integration ratio of coordinated to end-capped phosphines is 50 ± 10. The molecular weight is therefore calculated as 55 000 ± 11 000.

Poly-[Pt^{II}[1,2,4,5-tetrakis(diphenylphosphino)benzene]]$_{23}(BF_4)_{46}$ (1c). Tetrafluoroboric acid (0.14 mL of an 85% solution in ether) was added via syringe to a solution of (COD)$PtCl_2$ (250 mg, 0.67 mmol) in 15 mL of CH_2Cl_2. After the resulting solution had been stirred for 5 min, a solution of tppb (544 mg, 0.67 mmol) in 40 mL of CH_2Cl_2 was added. After the resulting solution was stirred for 12 h at room temperature, the solid product was collected by filtration and washed with CH_2Cl_2. Yield: 460 mg (58%). Anal. Calcd for $(C_{54}H_{42}P_4PtB_2F_8)_{23}$: C, 54.80; H, 3.58. Found: C, 53.45; H, 3.70.

End-group analysis was performed as with **1a**. After the suspension (437 mg of finely grounded polymer and 190 mg of tppb in 150 mL of CH_2Cl_2) had been stirred for 16 h at room temperature, the solid product was collected by filtration and washed with CH_2Cl_2. ^{31}P-NMR (DMSO-d_6): δ 42 (coordinated, $^1J_{^{195}Pt-P}$ = 2438 Hz), –14 (end-capped). The integration ratio of coordinated to end-capped phosphines is 23 ± 5. The molecular weight is therefore calculated as 27 000 ± 6000.

Bis[1,2-bis(diphenylphosphino)benzene]platinum(II) Tetrafluoroborate, [Pt(dppb)$_2$](BF$_4$)$_2$ (2c). A mixture of dppb (645 mg, 1.45 mmol) and K_2PtCl_4 (300 mg, 0.72 mmol) in 15 mL of H_2O and 35 mL of DMF was heated under reflux for 0.5 h. After the solution had been concentrated to ca. 15 mL under N_2, ether was added to induce precipitation of a solid product. The solid was collected by filtration and redissolved in 50 mL of CH_2Cl_2. To this solution was added HBF_4 (0.3 mL of an 85% solution in ether) via syringe. After the mixture had been stirred for 10 min at room temperature, MeOH was added to induce crystallization. The solid product was collected by filtration and was vacuum-dried. Yield: 370 mg (41%). ^{31}P-NMR (CD_3NO_2): δ 47.3 (t, $^1J_{^{195}Pt-P}$ = 2328 Hz). Anal. Calcd for $C_{60}H_{48}P_4PtB_2F_8$: C, 57.12; H, 3.83. Found: C, 56.66; H, 3.69.

[1,2-Bis(diphenylphosphino)benzene][1,3-bis(diphenylphosphino)propane] palladium(II) Tetrafluoroborate, [Pd(dppb)(dppp)](BF$_4$)$_2$] (3). A solution of dppp (186 mg, 0.45 mmol) in 20 mL of CH_2Cl_2 was added to a stirred solution of $[Pd(CH_3CN)_4](BF_4)_2$ (200 mg, 0.45 mmol) in 20 mL of CH_3CN. After the mixture had been stirred for 1 h at room temperature, a solution of dppb (201 mg, 0.45 mmol) in 15 mL of CH_2Cl_2 was added. The resulting mixture was stirred for 2 h before the solution was concentrated to ca. 10 mL under reduced pressure. The solid product was collected by filtration and was recrystallized from CH_3-

(9) Marcus, R. A.; Sutin, N. *Inorg. Chem.* **1975**, *14*, 213.
(10) Bard, A. J.; Faulkner, L. R. *Electrochemical Methods: Fundamentals and Applications;* Wiley: New York, 1980; p 701.
(11) Christina, H.; McFarlane, E.; McFarlane, W. *Polyhedron* **1988**, 1875.
(12) Sen, A.; Ta-Wang, L. *J. Am. Chem. Soc.* **1981**, *103*, 4627.
(13) Ittel, S. D. In *Inorganic Synthesis;* MacDiarmid, A. G., Ed.; McGraw-Hill: New York, 1977; Vol. 17, p 117.
(14) Levason, W.; McAuliffe, C. A. *Inorg. Chim. Acta* **1974**, *11*, 33.
(15) Levason, W.; McAuliffe, C. A. *Inorg. Chim. Acta* **1976**, *16*, 167.
(16) Miedaner, A.; Haltiwanger, R. C.; Dubois, D. L. *Inorg. Chem.* **1991**, *30*, 417.

NO_2/ether. Yield: 300 mg (58%). ^{31}P-NMR (CD_3CN): δ 56.3 (d, $^2J_{P-P'}$ = 303 Hz, 4P), −1.8 (d, $^2J_{P-P'}$ = 303 Hz, 4P).[17] Anal. Calcd for $C_{57}H_{50}P_4PdB_2F_8$: C, 60.11; H, 4.42. Found: C, 59.38 ; H, 4.60.

[1,2-Bis(diphenylphosphino)benzene][1,2,4,5-tetrakis(diphenylphosphino)benzene]nickel(II) Tetrafluoroborate, [Ni(dppb)(tppb)](BF$_4$)$_2$ (4). Tetrafluoroboric acid (0.19 mL of an 85% solution in ether) was added via syringe to a solution of (dppb)$NiCl_2$ (250 mg, 0.43 mmol) and tppb (353 mg, 0.43 mmol) in 200 mL of CH_2Cl_2. The resulting solution was stirred for 15 min at room temperature before the solution was concentrated to ca. 25 mL under reduced pressure. Ether was added to the filtrate in order to induce crystallization of the product. A solid product was collected by filtration and was recrystallized from CH_3NO_2/ ether. Yield: 325 mg (50%). ^{31}P-NMR (CD_3NO_2): δ 59.4 (m, 4P), −12.1(s, 2P). Anal. Calcd for $C_{84}H_{66}P_6NiB_2F_8$: C, 67.55; H, 4.45. Found: C, 66.12; H, 4.64.

[1,2-Bis(diphenylphosphino)benzene]M^{II}–1,2,4,5-tetrakis(diphenylphosphino)benzene–M^{II}[1,2-bis(diphenylphosphino)benzene] Tetrafluoroborate, [(dppb)M–tppb–M(dppb)](BF$_4$)$_4$ (M = Ni, Pd, Pt) (5a–c). Tetrafluoroboric acid (3 equiv) was added via syringe to a solution of (dppb)MCl_2 (M = Ni, Pd, Pt) (2 equiv) and tppb (1 equiv) in 200 mL of CH_2Cl_2. The resulting mixture was stirred for 5 min before the solution was concentrated to ca. 25 mL under reduced pressure. The solid product was collected by filtration and was recrystallized from CH_3NO_2/ether.

5a. Yield: 75%. ^{31}P-NMR (CD_3NO_2): δ 61.3 (m, 4P), 58.4 (m, 4P).[19] Anal. Calcd for $C_{114}H_{90}P_8Ni_2B_4F_{16}$: C, 63.03; H, 4.18. Found: C, 61.03; H, 3.91.

5b. Yield: 75%. ^{31}P-NMR (CD_3NO_2): δ 57.4 (m, 4P), 50.3 (m, 4P).[19] Anal. Calcd for $C_{114}H_{90}P_8Pd_2B_4F_{16}$: C, 60.38; H, 4.00. Found: C, 59.46; H, 3.99.

5c. Yield: 73%. ^{31}P-NMR (CD_3NO_2): δ 47.6 (m, $^1J_{^{195}Pt-P}$ = 2340 Hz, 4P), 44.2 (m, $^1J_{^{195}Pt-P}$ = 2340 Hz, 4P).[19] Anal. Calcd for $C_{114}H_{90}P_8Pt_2B_4F_{16}$: C, 56.00; H, 3.71. Found: C, 54.49; H, 3.72.

[1,2-Bis(diphenylphosphino)benzene]M$^{II}_1$–1,2,4,5-tetrakis(diphenylphosphino)benzene–M$^{II}_2$[1,2-bis(diphenylphosphino)benzene] Tetrafluoroborate, [(dppb)M$_1$–tppb–M$_2$(dppb)](BF$_4$)$_4$ (5d,e). Tetrafluoroboric acid (3 equiv of an 85% solution in ether) was added via syringe to a solution of [Ni(dppb)(tppb)](BF$_4$)$_2$ (1 equiv) and (dppb)MCl_2 (M = Pd, Pt) (1 equiv) in 200 mL of CH_2Cl_2. The resulting mixture was stirred for 5 min before the solution was concentrated to ca. 25 mL under reduced pressure. The solid product was collected by filtration and was recrystallized from CH_3NO_2/ether.

5d. Yield: 86%. ^{31}P-NMR (CD_3NO_2): Ni^{II}-coordinated phosphines, δ 60.4 (m, 2P), 57.3 (m, 2P); Pd^{II}-coordinated phosphines, δ 57.0 (m, 2P), 52.9 (m, 2P). Anal. Calcd for $C_{114}H_{90}P_8NiPdB_4F_{16}\cdot 4H_2O$: C, 59.74; H, 4.31. Found: C, 59.11; H, 4.00.

5e. Yield: 55%. ^{31}P-NMR (CD_3NO_2): Ni^{II}-coordinated phosphines, δ 61.1 (m, 2P), 59.8 (m, 2P); Pt^{II}-coordinated phosphines, δ 46.6 (m, 4P). Anal. Calcd for $C_{114}H_{90}P_8NiPtB_8F_{16}\cdot 4H_2O$: C, 57.51; H, 3.69. Found: C, 56.66; H, 3.69.

[1,3-Bis(diphenylphosphino)propane]Pd^{II}–1,2,4,5-tetrakis(diphenylphosphino)benzene]–Pd^{II}[1,3-bis(diphenylphosphino)propane] Tetrafluoroborate, [(dppp)Pd–tppb–Pd(dppp)](BF$_4$)$_4$ (6). A solution of dppp (186 mg, 0.45 mmol) in 20 mL of CH_2Cl_2 was added to a solution of [Pd(CH_3CN)$_4$](BF$_4$)$_2$ (200 mg, 0.45 mmol) in 20 mL of CH_3CN. After the mixture had been stirred for 1 h at room temperature, a solution of tppb (183 mg, 0.225 mmol) in 20 mL of $CHCl_3$ was added. The resulting mixture was stirred for 1 h before the solvent was removed under reduced pressure. The solid product was collected and was recrystallized from CH_2Cl_2/ether. Yield: 247 mg (50%). ^{31}P-NMR (CD_3CN): δ 50.4 (m, 4P), −1.6 (m, 4P). Anal. Calcd for $C_{108}H_{94}P_8Pd_2B_4F_{16}$: C, 58.97; H, 4.31. Found: C, 57.94; H, 4.09.

Electrochemical Reductive Doping of 1a, 1b, or 1c. A two-compartment electrochemical cell was rendered free of air and moisture by flushing with N_2 while the vessel was externally heated with a heat gun. The cell was equipped with a Pt flag as working electrode, a carbon cloth as counter electrode, and SCE as reference electrode. To the cathodic compartment was added **1a** (100 mg, 2.6×10^{-3} mmol), **1b** (60 mg, 1.1×10^{-3} mmol), or **1c** (300 mg, 1.1×10^{-2} mmol) in 40 mL of 0.1 M (TBA)PF_6/CH_3NO_2, 35 mL of 0.1 M (TBA)PF_6/DMSO, or 26 mL 0.1 M (TBA)PF_6/ DMSO, respectively. The electrolysis was conducted at −0.5, −0.75, or −0.8 V, and the reduction was halted after −3.7 C (0.20 equiv), −2.6 C (0.25 equiv), or −16.8 C (0.34 equiv) had passed, respectively. After the solvent in the cathodic compartment had been removed under vacuum, the solid product was collected, washed with deoxygenated THF, and vacuum-dried. The partially reduced **1a** (Ni^{II}–Ni^{I}) exhibited a five-line electron spin resonance spectrum (J = 73 G, g_{av} = 2.05) in CH_3NO_2. ^{31}P-NMR (DMSO-d_6) of the partially reduced **1b** (Pd^{II}–Pd^{0}): δ 50 (br), 35 (br).[20] The degree of doping, determined by the integration ratio of Pd^{II}-coordinated phosphines to Pd^{0}-coordinated phosphines, is 22%. ^{31}P-NMR (DMSO-d_6) of the partially reduced **1c** (Pt^{II}–Pt^{0}): δ 40 (br), 35 (br).[20] The degree of doping, determined by the integration ratio of Pt^{II}-coordinated phosphines to Pt^{0}-coordinated phosphines, is 20%.

Chemical Reductive Doping of 1a, 1b, or 1c. 4-Nitrobenzonitrile (NBN) radical anion (generated from bulk electrolysis of NBN at −1.0 V vs SCE) was added to **1a** (150 mg, 3.8×10^{-3} mmol), **1b** (150 mg, 2.7×10^{-3} mmol) , or **1c** (200 mg, 7.4×10^{-3} mmol). The concentration of NBN radical anion was 0.08 mmol in 20 mL of 0.1 M (TBA)PF_6/CH_2Cl_2, 0.08 mmol in 20 mL of (TBA)PF_6/CH_3CN, or 0.1 mmol in 25 mL of 0.1 M (TBA)PF_6/CH_3CN, respectively. After the resulting mixture had been stirred for 2 h, the solid product was collected by Schlenk filtration and washed with deoxygenated THF. The partially reduced **1a** (Ni^{II}–Ni^{I}) exhibited a five-line electron spin resonance spectrum (J = 73 G, g_{av} = 2.05) in CH_3NO_2. ^{31}P-NMR (DMSO-d_6) of the partially reduced **1b** (Pd^{II}–Pd^{0}): δ 50 (br), 35 (br).[20] The degree of doping, determined by the integration ratio of Pd^{II}-coordinated phosphines to Pd^{0}-coordinated phosphines, is 21%. ^{31}P-NMR (DMSO-d_6) of the partially reduced **1c** (Pt^{II}–Pt^{0}): δ 40 (br), 35 (br).[20] The degree of doping, determined by the integration ratio of Pt^{II}-coordinated phosphines to Pt^{0}-coordinated phosphnies, is 17%.

Results and Discussion

Electronic Effects. Table 1 summarizes redox potentials of complexes **2–6**. The monometallic complex **2a** shows two reversible one-electron reductions in acetonitrile. Dimetallic complex **5a** shows three slightly less cathodic reversible redox waves (Figure 1), the first being a two-electron wave and the second and third being one-electron waves (eq 1). The direct

$$\mathbf{5a}\ (Ni^{II}\text{–}Ni^{II}) \xrightarrow{2e^-} \mathbf{5a}\ (Ni^{I}\text{–}Ni^{I}) \xrightarrow{1e^-} \mathbf{5a}\ (Ni^{I}\text{–}Ni^{0}) \xrightarrow{1e^-} \mathbf{5a}\ (Ni^{0}\text{–}Ni^{0}) \quad (1)$$

reduction of the dimetallic complex **5a** to the corresponding Ni^{I}–Ni^{I} complex at approximately the same potential for the one-electron reduction of **2a** (Ni$^{II/I}$) indicates little interaction between the nickel centers in the dimetalated complex. (The assignment of the first reduction wave of the Ni^{II}–Ni^{II} complex as a two-electron conversion to the Ni^{I}–Ni^{I} complex is based on the similarity of the ESR and near-IR spectra of the reduced product to those of **2a**, Ni^{I}). The further reductions take place at potentials slightly less negative than that for the Ni$^{I/0}$ reduction of **2a**.

Somewhat different electrochemical behavior is observed with the corresponding Pd^{II} and Pt^{II} complexes. Thus, both the monometallic complexes **2b** and **2c** and the dimetalated complexes **5b** and **5c** show two-electron reduction waves in CH_3CN (Table 1). The latter complexes exhibit two reversible two-electron reduction waves (Figure 2 and 3). The nearly ideal reversibility of these two-electron reductions is shown by the expected magnitude of the peak-to-peak separation in the cyclic voltammetric waves. Unlike for the nickel complexes, the presence of a second metal causes a shift in the first reduction peak to a

(17) The downfield shift of dppb (56.3 ppm) or tppb (50.4 ppm) compared with dppp (−1.8 or −1.6 ppm) in **3** or **6**, respectively, is due to the different bite sizes involving the Pd.[16] The only coupling constant observed in the ^{31}P-NMR is assigned as trans[18] (the cis-coupling constant is not resolved). Similar ^{31}P-NMR spectra were reported for [Pd(dppb)$_2$](BF$_4$)$_2$ (52.6 ppm) and [Pd(dppp)$_2$](BF$_4$)$_2$ (0.0 ppm).[16]

(18) Verkade, J. G., Quin, L. D., Eds. *Phosphorus-31 NMR Spectroscopy in Stereochemical Analysis*; VCH Publishers: Deerfield Beach, FL, 1987; p 531.

(19) In general, the ^{31}P-NMR showed second-order spectra with one trans- and several cis-coupling constants being observed. It has been demonstrated that the computer simulation is necessary to derive the coupling constants in the similar second-order spectra of Ni^{II} and Pd^{II} phosphine complexes.[16]

(20) δ of the partially reduced **1b** (Pd^{II}–Pd^{0}): 50 (Pd^{II}-coordinated phosphines), 35 (Pd^{0}-coordinated phosphines). δ of the partially reduced **1c** (Pt^{II}–Pt^{0}): 40 (Pt^{II}-coordinated phosphines), 35 (Pt^{0}-coordinated phosphines).

Table 1. Cyclic Voltammetric Peak Potentials for the Reduction[a] of Several Mono- and Dimetallic Complexes

	potentials (V vs SCE)			
complex	$E_{1/2}$ (ΔE_p)[b]	$E_{1/2}$ (ΔE_p)[b]	$E_{1/2}$ (ΔE_p)[b]	K_c[c]
2a[16]	–0.26 (60 mV)	–0.60 (60 mV)		
	1e⁻ ($Ni^{II/I}$)	1e⁻ ($Ni^{I/0}$)		
2b[16]	–0.68 (40 mV)			
	2e⁻ ($Pd^{II/0}$)			
2c	–0.78 (40 mV)			
	2e⁻ ($Pt^{II/0}$)			
3	–0.63 (40 mV)			
	2e⁻ ($Pd^{II/0}$)			
4	–0.24 (70 mV)	–0.54 (70 mV)		
	1e⁻ ($Ni^{II/I}$)	1e⁻ ($Ni^{I/0}$)		
5a	–0.20 (80 mV)	–0.47 (60 mV)	–0.56 (40 mV)	42
	2e⁻ ($Ni^{II/I}$,$Ni^{II/I}$)	1e⁻ ($Ni^{I/0}$,Ni^{I})	1e⁻ (Ni^{0},$Ni^{I/0}$)	
5b	–0.56 (30 mV)	–0.67 (40 mV)		2×10^7
	2e⁻ ($Pd^{II/0}$,Pd^{II})	2e⁻ (Pd^{0},$Pd^{II/0}$)		
5c	–0.65 (30 mV)	–0.77 (40 mV)		3.7×10^7
	2e⁻ ($Pt^{II/0}$,Pt^{II})	2e⁻ (Pt^{0},$Pt^{II/0}$)		
5d	–0.18 (60 mV)	–0.41 (60 MV)	–0.66 (30 mV)	
	–0.18 (60 mV)[d]	–0.54 (60 mV)[d]	–0.74 (60 mV)[d]	
	1e⁻ ($Ni^{II/I}$,Pd^{II})	1e⁻ ($Ni^{I/0}$,Pd^{II})	2e⁻ (Ni^{0},$Pd^{II/0}$)	
5e	–0.17 (60 mV)	–0.41 (60 mV)	–0.83 (60 mV)	
	–0.18 (60 mV)[d]	–0.54 (60 mV)[d]	–0.92 (100 mV)[d]	
	1e⁻ ($Ni^{II/I}$,Pt^{II})	1e⁻ ($Ni^{I/0}$,Pt^{II})	2e⁻ (Ni^{0},$Pt^{II/0}$)	
6	–0.51 (40 mV)	–0.63 (40 mV)		2×10^8
	2e⁻ ($Pd^{II/0}$,Pd^{II})	2e⁻ (Pd^{0},$Pd^{II/0}$)		

[a] Reaction conditions: scan rate, 100 mV/s; reference electrode, Ag/AgCl; counter electrode, Pt wire; working electrode, Pt disk; 0.1 M tetrabutylammonium hexafluorophosphate in CH_3CN under N_2 at room temperature. [b] ΔE_p is the peak-to-peak separation between the cathodic and anodic waves. [c] K_c = comproportionation constant as described in eq 4. [d] Redox potential in CH_2Cl_2.

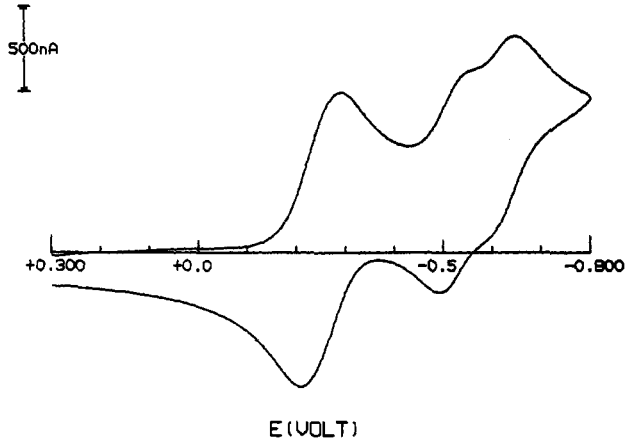

Figure 1. Cyclic voltammetry of **5a** (0.1 mM). Reaction conditions: scan rate, 100 mV/s; reference electrode, Ag/AgCl; counter electrode, Pt wire; working electrode, Pt disk; 0.1 M tetrabutylammonium hexafluorophosphate in CH_3CN under N_2 at room temperature.

somewhat less negative potential than is observed for the monometallic complexes **2b** and **2c**. The first two-electron reduction wave is shifted about 125 mV from that observed for the monometallic complexes, presumably because of the higher positive charge density in the dimetallic complexes. In both the monometallic and dimetallic complexes, rapid comproportionation of the M^IM^I complexes to the $M^{II}M^0$ complexes ($2M^I \rightarrow M^{II} + M^0$ and $2M^I\text{–}M^0 \rightarrow M^{II}\text{–}M^0 + M^0\text{–}M^0$) makes the observation of the former complexes impossible by the cyclic voltammetry, resulting in the two-step reduction shown in eq 2.

$$M^{II}\text{–}M^{II} \xrightarrow{2e^-} M^{II}\text{–}M^0 \xrightarrow{2e^-} M^0\text{–}M^0 \qquad (2)$$

The half-wave potential of the Pd^{II}/Pd^0 couple also shifts to a slightly less negative potential (about 50 mV) as the ligand is changed from dppb in **2b** and **5b** to dppp in **3** and **6**, respectively (Table 1). Because dppp has a larger bite size than dppb,[16] these

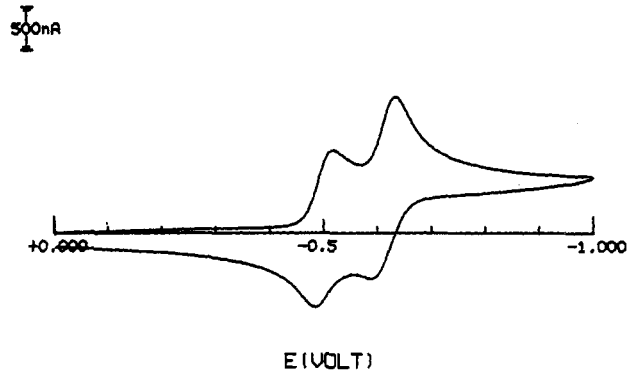

Figure 2. Cyclic voltammetry of **5b** (0.1 mM). Reaction conditions: scan rate, 100 mV/s; reference electrode, Ag/AgCl; counter electrode, Pt wire; working electrode, Pt disk; 0.1 M tetrabutylammonium hexafluorophosphate in CH_3CN under N_2 at room temperature.

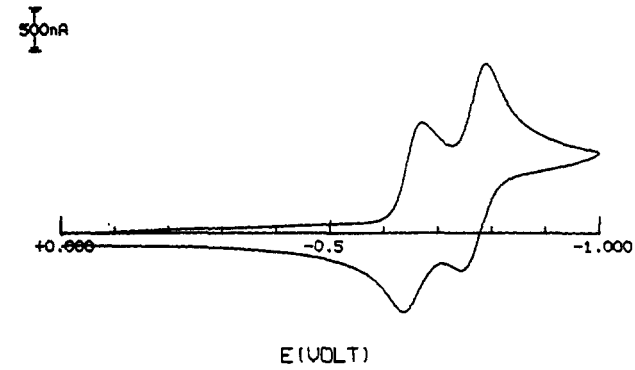

Figure 3. Cyclic voltammetry of **5c** (0.1 mM). Reaction conditions: scan rate, 100 mV/s; reference electrode, Ag/AgCl; counter electrode, Pt wire; working electrode, Pt disk; 0.1 M tetrabutylammonium hexafluorophosphate in CH_3CN under N_2 at room temperature.

shifts are consistent with an easier tetrahedral distortion of the Pd^{II} complexes in **3** and **6** than in **2b** and **5b**, thus facilitating the reduction of the square-planar Pd^{II} complex to the tetrahedral Pd^0 complex. A similar effect has been reported upon changing the ligand in [Ni^{II}(diphosphine)$_2$] complexes.[16]

The stability of mixed-valence dimetallic complexes **5** (Ni^I–Ni^0, Pd^{II}–Pd^0, Pt^{II}–Pt^0) can be expressed as K_c, the comproportionation constant, calculated as in eq 4. **A** represents the

$$\mathbf{A} \xrightarrow{n_1e^-,\,E_1^\circ} \mathbf{B} \xrightarrow{n_2e^-,\,E_2^\circ} \mathbf{C} \qquad (3)$$

$$K_c = \frac{[B]^{n_1+n_2}}{[C]^{n_1}[A]^{n_2}} = \exp\left[\frac{(E_1^\circ - E_2^\circ)n_1n_2F}{RT}\right] \qquad (4)$$

corresponding oxidized complexes **5** (Ni^I–Ni^I, Pd^{II}–Pd^{II}, Pt^{II}–Pt^{II}), **B** the mixed-valence complexes **5** (Ni^I–Ni^0, Pd^{II}–Pd^0, Pt^{II}–Pt^0), and **C** the reduced complexes **5** (Ni^0–Ni^0, Pd^0–Pd^0, Pt^0–Pt^0), respectively, n_1 and n_2 are the number of electrons transferred in each redox reaction, and F is Faraday's constant. The comproportionation constant K_c for dimetalated mixed-valence complexes calculated from the redox potentials E_1° and E_2° of the **A**/**B** and **B**/**C** couples[21] are summarized in Table 1. The K_c of **5b** (Pd^{II}-Pd^0) and **5c** (Pt^{II}–Pt^0) is approximately 10^6 times higher than that of **5a** (Ni^I–Ni^0). This is due to the two-electron comproportionation of **5b** (Pd^{II}–Pd^0) or **5c** (Pt^{II}–Pt^0), while only one-electron transfer is involved in the comproportionation of **5a** (Ni^{II}–Ni^0).

Geometry Effects. A geometry change normally takes place upon electrochemical reduction of d^8-transition-metal–phosphine complexes. The structures of [M^{II}(dppb)$_2$]X_2 (X = ClO_4, BF_4;

(21) Richardson, D. E.; Taube, H. *Inorg. Chem.* **1981**, *20*, 1278.

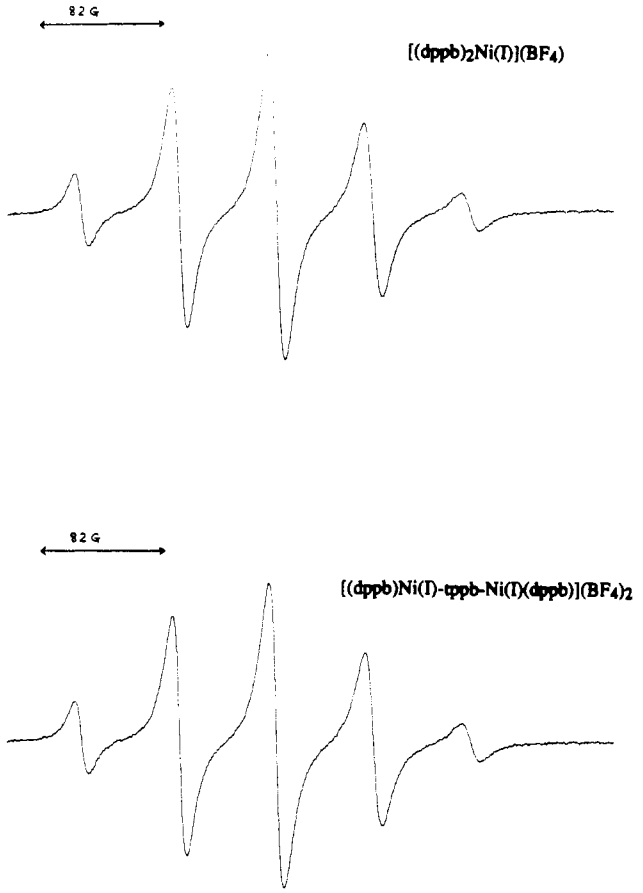

Figure 4. ESR spectra of electrochemically generated Ni^{I} complexes in deoxygenated CH_2Cl_2: (top) **2a**, Ni^{I} (0.2 mM); (bottom) **5a**, Ni^{I}–Ni^{I} (0.2 mM).

M = Ni, Pd, Pt) are usually square planar,[15,16,22] and the corresponding reduced complexes $[M^0(dppb)_2]$ (d^{10} configuration) are often tetrahedral because the geometry is dominated by steric effects in the absence of crystal field stabilization of the square-planar complex.[23] For example, an analogous square-planar complex $[Ni^{II}(depb)_2]$ (depb = 1,2-bis(diethylphosphino)benzene) becomes tetrahedral upon reduction, the formation of an intermediate Ni^{I} complex with a "square-planar-to-tetrahedral" geometry being observed.[24] In order to understand the geometry change accompanying the electrochemical reduction of mono- and dimetallic complexes **2a** and **5a**, the electrochemically generated Ni^{I} complexes were investigated by ESR and near-IR spectroscopies.

Controlled-potential bulk electrolyses of **2a** at –0.45 V and the corresponding dimetallic complex **5a** at –0.25 V resulted in the passage of 1.0 and 2.0 faradays/mol, respectively. Identical electron spin resonance spectra in CH_2Cl_2 are obtained for the monoreduced **2a** (Ni^{I}) and **5a** (Ni^{I}–Ni^{I}) (Figure 4). The observed five-line pattern (J = 64 G, g_{av} = 2.07) is attributed to the hyperfine coupling of Ni^{I} to the four symmetrically disposed phosphorus atoms arranged in a square-planar geometry about the metal, with the unpaired electron (d^9 configuration) occupying a $d_{x^2-y^2}$ orbital (HOMO). Moreover, an identical ESR spectrum is observed for **5a** (Ni^{I}–Ni^{I}) indicating that the two unpaired electrons (d^9–d^9 configuration) behave as localized electrons with minimal cross-ring metal–metal coupling since each Ni^{I} center is coupled to only four phosphorus atoms. A similar ESR spectrum has been reported for $[Ni^{I}(dppe)_2](BF_4)$ (dppe = 1,2-bis(diphenylphosphino)ethane).[25] In contrast to this square-planar Ni^{I} complex, a tetrahedral $Ni^{I}(PMe_3)_4$ complex has been reported to exhibit a broad ESR signal with no ^{31}P hyperfine structure.[26]

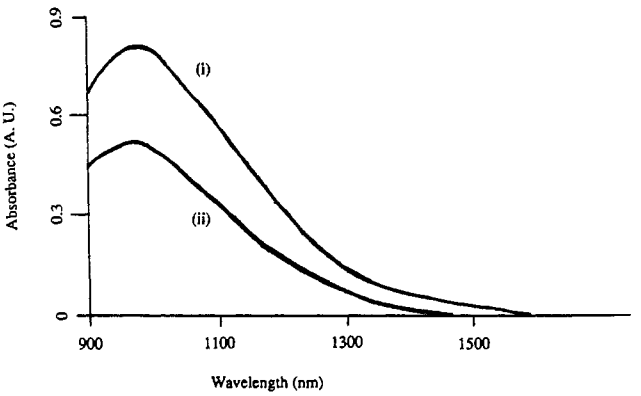

Figure 5. Near-IR absorption spectra of electrochemically generated Ni^{I} complexes in deoxygenated CH_2Cl_2: (i) **2a**, Ni^{I} (3.1 mM); (ii) **5a**, Ni^{I}–Ni^{I} (1.1 mM).

Near-IR absorptions are observed at 978 nm (ϵ = 270 M^{-1} cm^{-1}) for **2a** (Ni^{I}) and at 968 nm (ϵ = 460 M^{-1} cm^{-1}) for **5a** (Ni^{I}–Ni^{I}) (Figure 5). The observed red shift of the d–d transition[27] for **2a** (Ni^{I}) and **5a** (Ni^{I}–Ni^{I}) compared with that for **2a** (Ni^{II}) and **5a** (Ni^{II}–Ni^{II}) suggests a smaller energy gap between the nonbonding (d_{z^2}) and antibonding orbitals ($d_{x^2-y^2}$) in the reduced complexes. The energy of the unpaired electron ($d_{x^2-y^2}$ orbital) is significantly lower in a tetrahedrally distorted square-planar Ni^{I} complex than in the corresponding Ni^{II} complex because the phosphorus σ orbitals in a tetrahedral complex interact less strongly with nickel than they do in a square planar geometry,[23] as has been established with molecular orbital calculations for $[Ni(PH_3)_4]^{2+}$ and $[Ni(PH_3)_4]^{+}$.[16] Thus, the ESR and near-IR spectral data suggest that **2a** (Ni^{I}) and **5a** (Ni^{I}–Ni^{I}) have the same geometry (a tetrahedrally distorted square-planar structure).

Intervalence Charge Transfer. Three reversible redox waves (eq 5) are observed for the heterodimetallic complexes **5d** and **5e**,

$$Ni^{II}\text{–}M^{II} \xrightarrow{1e^-} Ni^{I}\text{–}M^{II} \xrightarrow{1e^-} Ni^{0}\text{–}M^{II} \xrightarrow{2e^-} Ni^{0}\text{–}M^{0} \qquad (5)$$

the first and second being one-electron waves and the third being a two-electron wave (Table 1). Because the onsets of the first reduction waves of **5d** and **5e** more closely mimic that of the dimetallic complex **5a** than the corresponding palladium (**5b**) or platinum (**5c**) complexes, we assume that the Ni^{0}–M^{II} (M = Pd, Pt) oxidation state is attained after the two sequential one-electron reductions. The corresponding mixed-valence dimetallic complexes **5d** (Ni^{0}–Pd^{II}) and **5e** (Ni^{0}–Pt^{II}), generated by bulk electrolysis at –0.5 V, exhibit broad absorption bands at 602 nm (ϵ = 1000 M^{-1} cm^{-1}) for **5d** (Ni^{0}–Pd^{II}) and at 618 nm (ϵ = 2200 M^{-1} cm^{-1}) for **5e** (Ni^{0}–Pt^{II}). These bands are assigned as intervalence charge transfer (IT) bands[28] and are absent in the spectra of both the fully oxidized Ni^{II}–M^{II} and fully reduced Ni^{0}–M^{0} complexes (Figures 6 and 7). For the homometallic complexes **5a–c** and **6**, IT bands are observed at 704 nm (ϵ = 700 M^{-1} cm^{-1}) for the mixed-valence complexes **5c** (Pt^{II}–Pt^{0}) and at 500 nm (ϵ = 3600 M^{-1} cm^{-1}) for the **6** (Pd^{II}–Pd^{0}).

Marcus and Hush have established models that relate the rates of optical and thermal electron transfer in mixed-valence transition

(22) Levason, W.; McAuliffe, C. A. *J. Chem. Soc., Dalton. Trans.* **1974**, 2238.
(23) Huheey, J. E. *Inorganic Chemistry: Principles of Structure and Reactivity*; Harper & Row Publishers: New York, 1983; p 359.
(24) Fox, M. A.; Chandler, D. A.; Kyba, E. P. *J. Coord. Chem.* **1992**, *25*, 1.
(25) Bowmaker, G. A.; Boyd, P. D. W.; Campbell, G. K.; Hope, J. M. *Inorg. Chem.* **1982**, *21*, 1152.
(26) Gleizes, A.; Dartiguenave, M.; Dartiguenave, Y.; Galy, J.; Klein, H. F. *J. Am. Chem. Soc.* **1977**, *99*, 5187.
(27) The d–d transition is shifted from 432 nm in **2a** to 978 nm in the corresponding Ni^{I} complex and from 430 nm in **4a** to 968 nm in the corresponding Ni^{I}–Ni^{I} complex.
(28) Hush, N. S. *Prog. Inorg. Chem.* **1967**, *8*, 357.

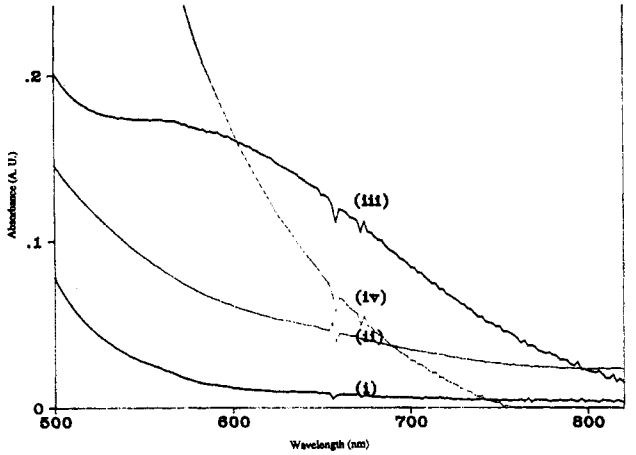

Figure 6. Absorption spectra of **5d** (0.14 mM) at different oxidation states in deoxygenated CH_2Cl_2: (i) **5d**, Ni^{II}–Pd^{II}; (ii) **5d**, Ni^{I}–Pd^{II}; (iii) **5d**, Ni^{0}–Pd^{II}; (iv) **5d**, Ni^{0}–Pd^{0}. Deconvolution of spectrum iii reveals a maximum at 602 nm.

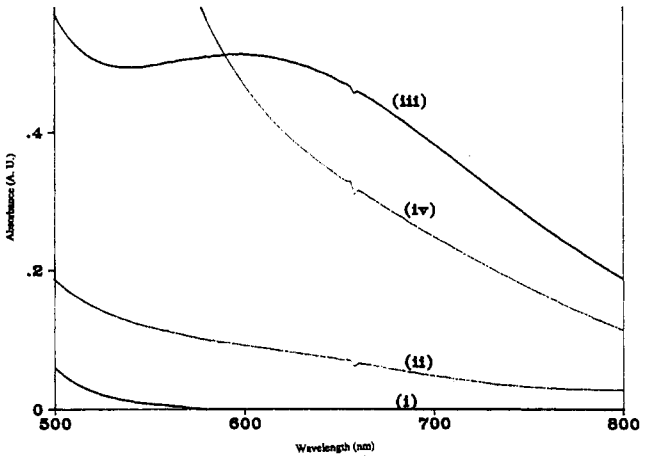

Figure 7. Absorption spectra of **5e** (0.22 mM) at different oxidation states in deoxygenated CH_2Cl_2: (i) **5e**, Ni^{II}–Pt^{II}; (ii) **5e**, Ni^{I}–Pt^{II}; (iii) **5e**, Ni^{0}–Pt^{II}; (iv) **5e**, Ni^{0}–Pt^{0}. Deconvolution of spectrum iii reveals a maximum at 618 nm.

metal complexes to the IT absorption maximum for a one-electron intervalence charge transfer.[29] Systems with two-electron oxidation-state change have also been examined, e.g., Wolffram's red salt Pt^{II}–Pt^{IV}, and a three-potential well energy diagram was employed to describe the resulting intermetallic electronic coupling in which single-electron optical charge transfer from Pt^{II} to Pt^{IV} leads to the formation of a metastable Pt^{III}–Pt^{III} complex.[30] More recently, Bocarsly used an analogous energy diagram to describe electronic interaction in a Fe^{II}–Pt^{IV}–Fe^{II} trimeric complex.[31]

Thermal and optical electron transfer in mixed-valence complexes **5d** (Ni^{0}–Pd^{II}) and **5e** (Ni^{0}–Pt^{II}) can be understood from the qualitative energy diagram shown in Figure 8. Similar potential energy diagram have been calculated for Wolffram's red salt Pt^{II}–Pt^{IV}.[32] Thermal electron transfer between the metal centers converts the initial Ni^{0}–M^{II} complex (**A**) into the Ni^{I}–M^{I} state (**B**) with an activation energy barrier E_a. This product complex is then converted by comproportionation to the Ni^{II}–M^{0} complex (**C**) or it can revert to the starting material, depending on the relative activation energy of each electron transfer. Photoinduced electron transfer involves optical excitation of **A** to produce an excited state **A***. **A*** can decay to **A**, **B**, or **C**, depending upon the proximity of surface-crossing points and the

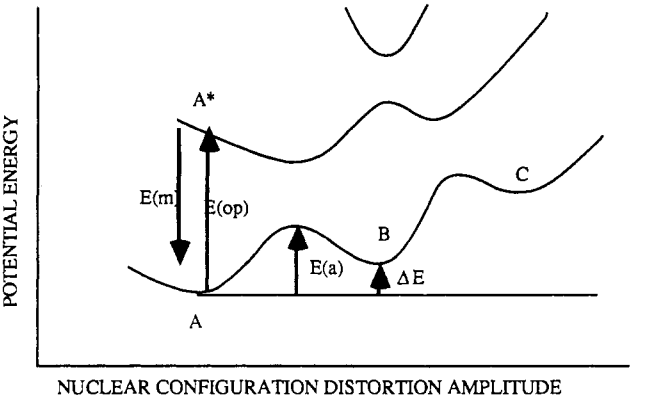

Figure 8. Qualitative schematic energy diagram[32] for optical and thermal electron transfer of **5d** (Ni^{0}–Pd^{0}) and **5e** (Ni^{0}–Pt^{0}) and related species: **A**, Ni^{0}–M^{II} (M = Pd or Pt); **A***, charge transfer excited state of **A**; **B**, metastable intermediate Ni^{I}–M^{I}; **C**, Ni^{II}–M^{0}; E_m, reorganization energy; E_{op}, maximum of the IT absorption band; E_a, thermal activation barrier; ΔE, free energy of the redox reaction in eq 7.

magnitude of electronic coupling at the critical geometries.[31] Thermodynamically, the reaction must produce the most stable species as the final product, although kinetic effects, in principle, could trap the dimetallic complex in a thermodynamically less stable state.

For an unsymmetrical mixed-valence dimer, the thermal and optical electron transfers are related by eq 6,[33] where E_{op} is the

$$E_{op} = E_m + \Delta E \tag{6}$$

maximum of the IT absorption band, E_m is the reorganization energy of the electron transfer, and ΔE is the free energy of the electron transfer in **5d** and **5e** as shown in eq 7 (M = Pd, Pt).

$$Ni^{0}\text{–}M^{II} \rightarrow Ni^{I}\text{–}M^{I} \tag{7}$$

The reduction potentials of the $Ni^{I/0}$ couple in **5d** and **5e** are –0.54 V. The reduction potentials of Ni^{0}–$M^{II/I}$ couple in **5d** and **5e** are –0.74 and –0.92 V, respectively, assuming that the observed reduction potential represents the $M^{II/I}$ couple and that the reduction of the $M^{I/0}$ couple occurs at a less negative potential. From the Nernst equation, ΔE of the redox reaction (eq 7) is calculated as 0.20 and 0.38 V for **5d** (Ni^{0}–Pd^{II}) and **5e** (Ni^{0}–Pt^{II}), respectively.[34] From known E_{op} and eq 6, the reorganization energies for intramolecular charge exchange (E_m) are calculated as 1.86 and 1.62 V for **5d** (Ni^{0}–Pd^{II}) and **5e** (Ni^{0}–Pt^{II}), respectively.[34]

The thermal activation barriers, E_a, can then be calculated from eq 8,[33] yielding values of 0.57 and 0.62 V for **5d** (Ni^{0}–Pd^{II})

$$E_a = \frac{E_{op}^{\,2}}{4(E_{op} - \Delta E)} \tag{8}$$

and **5e** (Ni^{0}–Pt^{II}), respectively.[34] The rate constants for thermal electron transfer can then be calculated from eq 9,[35] where k, the

$$k = k\nu_n \exp(-E_a/RT) \tag{9}$$

adiabaticity factor for electron transfer, is assumed to be 1, υ_n is the nuclear frequency factor (typically estimated to be $\sim 5 \times 10^{12}$ s^{-1}),[27] and E_a, calculated as in eq 8, is used to approximate ΔG^*, the thermal activation energy. Electron transfer rate constants are then calculated as 1150 s^{-1} for **5d** (Ni^{0}–Pd^{II}) and 160 s^{-1} for **5e** (Ni^{0}–Pt^{II}) at 298 K (Table 2.)[34]

(29) Hush, N. S. *Prog. Inorg. Chem.* **1967**, *8*, 391.
(30) Keiichiro, N. *J. Phys. Soc. Jpn.* **1984**, *53*, 427.
(31) Pfenning, B. W.; Bocarsly, A. B. *J. Phys. Chem.* **1992**, *96*, 226.
(32) Yoshiki, W.; Tadaoki, M.; Masahiro, Y.; Takao, K. *J. Phys. Soc. Jpn.* **1985**, *54*, 3143.
(33) Brown, D. B., Ed. *Mixed-Valence Compounds*; D. Reidel Publishing Co.: Dordrecht, Holland, 1980.
(34) See Appendix.
(35) Creutz, C. *Prog. Inorg. Chem.* **1989**, *30*, 1.

Table 2. Optical and Thermal Electron Transfer Parameters for Mixed-Valence Heterodimetallic Complexes **5**

complex	E_{op} (eV)[a]	ΔE (V)[b]	E_m (V)[c]	E_s (V)[d]	k (s^{-1})[e]
5d (Ni^0–Pd^{II})	2.06	0.20	1.86	0.57	1150
5e (Ni^0–Pt^{II})	2.00	0.38	1.62	0.62	160

[a] From the maximums of the observed IT bands of **5d** (Ni^0–Pd^{II}) and **5e**(Ni^0–Pt^{II}). [b] From cyclic voltammetric peak potentials of **5d** and **5e**, as discussed in text. [c] From eq 6. [d] From eq 8. [e] From eq 9.

Table 3. Solvent Dependence of the IT Bands of **5d** (Ni^0–Pd^{II}) and **5e** (Ni^0–Pt^{II})

	λ_{max} (nm) (E_{op} (eV)[a])		
solvent	**5d** (Ni^0–Pd^{II})	**5e** (Ni^0–Pt^{II})	$1/D_{op} - 1/D_s$[b]
CH_3CN	578 (2.15)	602 (2.06)	0.527
CH_3NO_2	594 (2.10)	606 (2.05)	0.497
CH_3COCH_3	583 (2.13)	608 (2.04)	0.493
CH_2Cl_2	602 (2.06)	618 (2.01)	0.383

[a] From the maximum of the observed IT band. [b] D_{op} and D_s are the optical and static dielectric constants of the solvents, respectively.

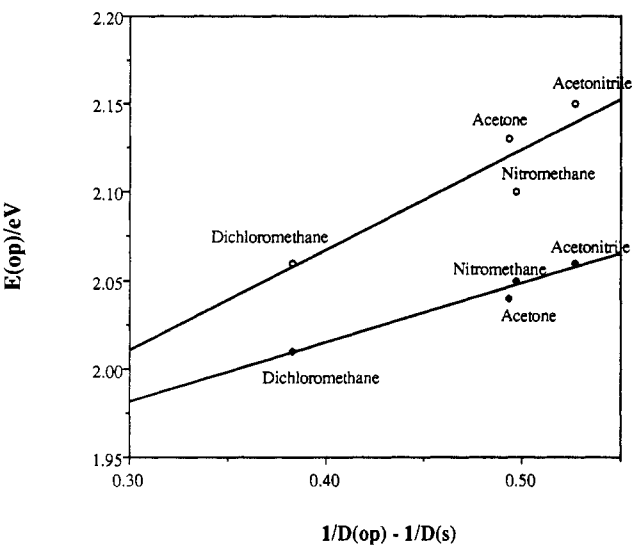

Figure 9. Dependence of E_{op} of (o) **5d** (Ni^0–Pd^0) and (•) **5e** (Ni^0–Pt^0) on the optical and static dielectric constants of solvents.

Meyer has shown that, for optical electron transfer in unsymmetrical mixed-valence complexes, the reorganization energy can be expressed as in eq 10,[33] where x_o and x_i are the

$$E_m = x_i + x_o = x_i + e^2\left(\frac{1}{2a_1} + \frac{1}{2a_2} - \frac{1}{r}\right)\left(\frac{1}{D_{op}} - \frac{1}{D_s}\right) \quad (10)$$

energy barriers for the outer-sphere and inner-sphere electron transfers, respectively, a_1 and a_2 are the metal–ligand bond lengths (in the different oxidation states of the metal centers) in the mixed-valence dimetallic complexes, r is the separation between the two interacting metal centers, and D_{op} and D_s are the optical and static dielectric constants of the solvents. Inserting eq 10 into eq 6 leads to the expectation of a linear plot of E_{op} vs $(1/D_{op} - 1/D_s)$ with an intercept of $(x_i + \Delta E)$. The solvent dependence of the IT maximum in **5d** (Ni^0–Pd^{II}) and **5e** (Ni^0–Pt^{II}) in several solvents is shown in Table 3. Plots of E_{op} against $1/D_{op} - 1/D_s$ (Figure 9) are linear with intercepts of 1.84 V for **5d** (Ni^0–Pd^{II}) and 1.88 V for **5e** (Ni^0–Pt^{II}). With ΔE equal to 0.20 and 0.38 V (eq 6), the energy barriers of inner-sphere electron transfer are calculated as 1.64 V for **5d** (Ni^0–Pd^{II}) and 1.5 V for **5e** (Ni^0–Pt^{II}).

The larger inner-sphere electron transfer energy barriers for **5d** (Ni^0–Pd^{II}) and **5e** (Ni^0–Pt^{II}) compared to the symmetrical Ru^{II}–L–Ru^{III} dimers (L = 4,4′-bipyridine, 4,4′-bipyridylethylene, etc.; 0.25–0.74 eV)[36] are due to two effects: (1) participation of the antibonding orbitals of the metal centers in **5d** (Ni^0–Pd^{II}) and **5e** (Ni^0–Pt^{II}); (2) geometry changes induced by electron transfer (square planar for M^{II} complexes; tetrahedrally distorted square planar for M^I complexes; tetrahedral for M^0 complexes).

Table 4. Conductivity[a] of the Metal Coordination Polymers **1a–c**

polymer	conductivity (Ω^{-1} cm^{-1})[b]
1a	$(7 \pm 2) \times 10^{-9}$
1b	$(2 \pm 1) \times 10^{-8}$
1c	$(8 \pm 7) \times 10^{-9}$
mixed-valence polymer **1a** (Ni^{II}–Ni^I)[c]	$<10^{-9}$
mixed-valence polymer **1a** (Pd^{II}–Pd^0)[c]	$<10^{-9}$
mixed-valence polymer **1c** (Pt^{II}–Pt^0)[c]	$<10^{-9}$

[a] Conductivity is measured by the two-probe technique[8] on a pressed powder sample in a sandwich cell with a thickness of ~1 mm. [b] Average of two measurements on independently prepared samples. [c] From electrochemical or chemical doping of **1a–c** (ca. 20%), as discussed in the text.

Conductivity Measurements of Metal Coordination Polymers. Conductivities of the coordination polymers **1a–c** measured as pressed powder samples in a sandwich cell with a two-probe technique[8] are summarized in Table 4. The low conductivity of these metal coordination polymers indicates that the transition metals in the M^{II} oxidation state are only weakly coupled along the polymer backbone. The mixed-valence polymer **1a** (Ni^{II}–Ni^I), **1b** (Pd^{II}–Pd^0), or **1c** (Pt^{II}–Pt^0), generated by electrochemical or chemical doping (~20% of metal centers in **1a, 1b,** or **1c** are reduced), exhibits a conductivity less than 10^{-9} $(\Omega\ cm)^{-1}$ (Table 4). The low conductivity of mixed-valence polymers **1a** (Ni^{II}–Ni^I), **1b** (Pd^{II}–Pd^0), and **1c** (Pt^{II}–Pt^0) suggests that the metal–metal interactions in the polymer backbone are disrupted because of the geometry change associated with the partial reduction of polymer.

The mixed-valence polymer **1c** (Pt^{II}–Pt^0) exhibits an IT absorption band at 629 nm, which is blue-shifted from that of the analogous dimetallic complex **5c** (Pt^{II}–Pt^0) (704 nm). The increased activation barrier of electron transfer in the mixed-valence polymer **1c** (Pt^{II}–Pt^0) is probably due to the rigidity of the polymer backbone, requiring a larger reorganization energy for the electron transfer. Similar behavior has been reported with the IT band of $(-Fe^{II}$–$Pt^{IV}-)_n$.[37] No intervalence charge transfer band was observed for mixed-valence polymers **1a** (Ni^{II}–Ni^I) and **1b** (Pd^{II}–Pd^0). Although model studies of mixed-valence dimetallic complexes **5d** (Ni^0–Pd^{II}) and **5e** (Ni^0–Pt^{II}) show enhanced intermetallic electronic coupling, the low conductivity of mixed-valence polymers **1a** (Ni^{II}–Ni^I), **1b** (Pd^{II}–Pd^0), and **1c** (Pt^{II}–Pt^0) indicates that the effect of enhanced electronic interactions in the partially reduced polymers is outweighed by an adverse geometric effect.

Conclusions

Much lower conductivities are observed in the metal coordination polymers **1a–c** than in the previously described metal–thiolene coordination polymers. The high delocalization in the ground state of the latter polymers arising from the interaction of the unpaired electrons on sulfur with a vacant d orbital of the metal ion[38] is not possible in the metal–phosphine complexes because of the absence of a noncoordinating electron pair in an accessible 3p orbital of the phosphine ligand. We conclude therefore that the low conductivity of **1** is caused by (1) low intermetallic electronic coupling through the tetrakis(diphenylphosphino)-benzene bridging ligand, (2) a large thermal activation energy

(36) (a) Powers, M. J.; Meyer, T. J. *J. Am. Chem. Soc.* **1980**, *102*, 1289. (b) Sullivan, B. P.; Meyer, T. J. *Inorg. Chem.* **1980**, *19*, 752. (c) Powers, M. J.; Meyer, T. J. *Inorg. Chem.* **1978**, *17*, 1785.
(37) Pfenning, B. W.; Bocarsly, A. B. *Coord. Chem. Rev.* **1991**, *111*, 91.
(38) Alcacer, L.; Novais, H. In *Extended Linear Chain Compounds;* Miller, J. S., Ed.; Plenum Press: New York, 1983; Vol. 3, p 319.

for electron transfer and, consequently, a slow electron transfer rate in the polymers, as evidenced by analogous effects in the dimetalated model complexes **5a–e**, and (3) a substantial geometry change that accompanies charge transfer along the polymer chain.

Acknowledgment. This work is supported by the Office of Basic Energy Sciences, U.S. Department of Energy. We thank Dr. Wayne Jones for helpful discussions and assistance in the preparation of the manuscript.

Appendix

(1) Free energy of electron transfer:

$$Ni^0\text{–}M^{II} \xrightarrow{\Delta E} Ni^{I}\text{–}M^{I}$$

$$\Delta E(\text{Ni–Pd}) = E(Ni^{0/I}) - E(Pd^{II/I})$$
$$= (-0.54\text{ V}) - (-0.74\text{ V})$$
$$= 0.20\text{ V for reversible system}$$

$$\Delta E(\text{Ni–Pt}) = E(Ni^{0/I}) - E(Pt^{II/I})$$
$$= (-0.54\text{ V}) - (-0.92\text{ V})$$
$$= 0.38\text{ V for reversible system}$$

(2) Reorganization energy E_m:

$$E_m(Ni^0\text{–}Pd^{II}) = E_{op}(Ni^0\text{–}Pd^{II}) - \Delta E(\text{Ni–Pd})$$
$$= 2.06\text{ V} - 0.20\text{ V} = 1.86\text{ V}$$

$$E_m(Ni^0\text{–}Pt^{II}) = E_{op}(Ni^0\text{–}Pt^{II}) - \Delta E(\text{Ni–Pt})$$
$$= 2.00\text{ V} - 0.38\text{ V} = 1.62\text{ V}$$

(3) Activation energy barrier E_a:

$$E_a(Ni^0\text{–}Pd^{II}) = \frac{E_{op}^2(Ni^0\text{–}Pd^{II})}{4(E_{op}(Ni^0\text{–}Pd^{II}) - \Delta E)}$$
$$= \frac{(2.06\text{ V})^2}{4(2.06\text{ V} - 0.20\text{ V})} = 0.57\text{ V}$$

$$E_a(Ni^0\text{–}Pt^{II}) = \frac{E_{op}^2(Ni^0\text{–}Pt^{II})}{4(E_{op}(Ni^0\text{–}Pt^{II}) - \Delta E)}$$
$$= \frac{(2.00\text{ V})^2}{4(2.00\text{ V} - 0.38\text{ V})} = 0.62\text{ V}$$

(4) Electron transfer rate constant k (from eq 9):

$$k(Ni^0\text{–}Pd^{II}) = 1150\text{ s}^{-1};\ k(Ni^0\text{–}Pt^{II}) = 160\text{ s}^{-1}$$